International Journal of Nanomedicine

Dovepress
open access to scientific and medical research

Open Access Full Text Article

ORIGINAL RESEARCH

Glypican-1-antibody-conjugated Gd–Au nanoclusters for FI/MRI dual-modal targeted detection of pancreatic cancer

This article was published in the following Dove Press journal:
International Journal of Nanomedicine

Xin Huang,[1,*] Chengqi Fan,[2,*] Huanhuan Zhu,[1] Wenjun Le,[1] Shaobin Cui,[1] Xin Chen,[3] Wei Li,[4] Fulei Zhang,[4] Yong Huang,[4] Donglu Shi,[1,5] Zheng Cui,[1,6] Chengwei Shao,[2] Bingdi Chen[1]

[1]The Institute for Translational Nanomedicine, Shanghai East Hospital, The Institute for Biomedical Engineering & Nano Science, Tongji University School of Medicine, Shanghai, China; [2]Radiology Department of Changhai Hospital, The Second Military Medical University, Shanghai, China; [3]Department of Thyroid Surgery, The First Bethune Hospital of Jilin University, Jilin, China; [4]International Joint Cancer Institute, The Second Military Medical University, Shanghai, China; [5]The Materials Science & Engineering Program, Department of Mechanical & Materials Engineering, College of Engineering & Applied Science, University of Cincinnati, OH, USA; [6]Department of Pathology, Wake Forest University School of Medicine, Winston-Salem, NC, USA

*These authors contributed equally to this work

Introduction: Pancreatic cancer (PC) has a poor prognosis with high mortality, due to the lack of effective early diagnostic and prognostic tools.

Materials and methods: In order to target and diagnose PC, we developed a dual-modal imaging probe using Glypican-1 (GPC-1) antibody conjugated with Gd–Au nanoclusters (NCs; Gd-Au-NC-GPC-1). GPC-1 is a type of cell surface heparan sulfate proteoglycan, which is often highly expressed in PC. The probe was successfully prepared with a hydrodynamic diameter ranging from 13.5 to 24.4 nm.

Results: Spectral characteristics showed absorption at 280 nm and prominent emission at 650 nm. Confocal microscopic imaging showed effective detection of GPC-1 highly expressed PC cells by Gd-Au-NC-GPC-1, which was consistent with flow cytometry results. In vitro relaxivity characterization demonstrated that the r1 value of the probe was 17.722 s^{-1} mM^{-1} Gd, which was almost 4 times higher compared with that of Gd-diethylenetriaminepentacetate (DTPA; r1 value =4.6 s^{-1} mM^{-1} Gd). Gd-Au-NC-GPC-1 exhibited similar magnetic resonance (MR) signals when compared to Gd-DTPA even at lower Gd concentrations. Much higher MR signals were registered in PC cells (COLO-357) compared with normal cells (293T). Furthermore, Gd-Au-NC-GPC-1 could effectively detect PC cells in vivo by dual-modal fluorescence imaging/magnetic resonance imaging (FI/MRI) at 30 minutes postinjection. In addition, Gd-Au-NC-GPC-1 did not show significant biotoxicity to normal cells at tested concentrations both in vitro and in vivo.

Conclusion: Gd-Au-NC-GPC-1 has demonstrated to be a promising dual-modal FI/MRI contrast agent for targeted diagnosis of PC.

Keywords: pancreatic cancer, Glypican-1, fluorescence imaging, magnetic resonance imaging, Gd–Au NCs

Introduction

Pancreatic cancer (PC) is considered to be one of the deadliest diseases. Its 5-year survival rate is <5%.[1,2] For most PC patients, the tumor lesions are not detected at an early stage, which explains the high mortality rate. Most PC patients do not show any significant symptoms until the cancer has already metastasized; consequently, surgical therapy is no longer effective.[3] Hence, there is an urgent need to develop clinical diagnostic tools for early detection and diagnosis, which could significantly improve prognosis and survival.[4–6]

For PC diagnosis, it is critical to discern specific biomarkers that are highly tumor-specific.[7] One of these biomarkers, carbohydrate antigen 19-9 (CA19-9), has been used in the clinic to screen PC patients. However, CA19-9 lacks specificity and sensitivity, making it unable to distinguish malignant tissues from benign tissues.[8–10] In 2015, Melo et al reported a potential biomarker for PC, Glypican-1 (GPC-1).[11] As a heparan sulfate

Correspondence: Bingdi Chen
The Institute for Translational Nanomedicine, Shanghai East Hospital, The Institute for Biomedical Engineering & Nano Science, Tongji University School of Medicine, No 1239, Siping Road, Shanghai, 200092, China
Tel/fax +86 21 6598 3706
Email inanochen@tongji.edu.cn

Chengwei Shao
Radiology Department of Changhai Hospital, The Second Military Medical University, No 168, Changhai Road, Shanghai, 200433, China
Tel/fax +86 21 3116 2148
Email cwshao@sina.com

submit your manuscript | www.dovepress.com
Dovepress
http://dx.doi.org/10.2147/IJN.S158559

proteoglycan on cell membrane, GPC-1 promotes tumor growth and invasion.[12,13] The expression of GPC-1 is higher in human PC compared with normal pancreatic or benign lesions, making it an ideal biomarker for PC detection.[12]

In recent years, multimodal molecular imaging has attracted researchers' attention for medical diagnosis. Using a combination of imaging systems, it is possible to monitor tumor biological behavior in real time and to analyze malignant tissue at the cellular and subcellular level. Currently, in both clinical and preclinical settings, positron emission tomography and single-photon emission computed tomography are considered the common approaches for functional imaging, while magnetic resonance imaging (MRI) and computed tomography are used for structural imaging. In addition, optical tools, including fluorescence imaging (FI) and bioluminescence imaging, have become popular because of their low cost.[14–17]

A variety of multimodal nanoprobes have been synthesized for molecular imaging in medical research.[18–22] Among them, dual-modal fluorescence imaging/magnetic resonance imaging (FI/MRI) agents exhibit impressive advantages and have attracted many researchers' attention for years. Both FI and MRI are noninvasive and nonradioactive, and so these two imaging methods are safe.[23] FI, operating at wavelengths >600 nm, offers high detection sensitivity (including low background and autofluorescence detection), but it is limited for spatial resolution.[23,24] In contrast, MRI does not have the shortcomings of shallow tissue penetration or poor image quality. It has high anatomical resolution, but lacks sensitivity.[25–27] Dual-modal FI/MRI integrates the advantages of both FI and MRI. Dual-modal FI/MRI agents exhibit desirable resolution, sensitivity, and penetration depth. These characteristics make dual-modal FI/MRI agents well suited to obtain precise information of tumor sites, in the clinic.

Herein, we report a dual-modal FI/MRI probe, Gd–Au nanoclusters (NCs) conjugated with GPC-1 antibody (Gd-Au-NC-GPC-1), for detecting PC cells. Gd-Au-NC-GPC-1 shows dual-modal imaging with intense red fluorescent emission and strong T1 effect. In addition, conjugation with GPC-1 antibody enables the functional imaging probe to target high-GPC-1-expressing PC cells both in vitro and in vivo.

Materials and methods

Reagents

All reagents were commercially available. Ultrapure water was obtained by Millipore machines (Billerica, MA, USA). The following are the manufacturer details of the reagents: Bovine serum albumin (BSA) was purchased from Sigma-Aldrich (Louis, MO, USA); $HAuCl_4$ from Guoyao Reagent Corporation (Shanghai, China); $GdCl_3{\cdot}6H_2O$ from HWRK Chemistry Corporation (Beijing, China); NaOH from Aladdin Chemistry Corporation (Shanghai, China); and 1-ethyl-3-(3-dimethylaminopropyl)carbodiimide (EDC)·HCl from GL Biochemistry Corporation (Shanghai, China).

Instrumentation

The following are the details of the instrumentation: Agilent 7800 (Hitachi Ltd., Tokyo, Japan) was used for inductively coupled plasma mass spectrometry; JEM-2100F electron microscopy (JEOL, Tokyo, Japan) for high-resolution transmission electron microscopy (HRTEM); Veeco Nano-Scope Multimode IIIa (Veeco, Plainview, NY, USA) for atomic force microscopy (AFM); JEM Zetasizer Nano-ZS90 (Malvern Instruments, Malvern, UK) for hydrodynamic diameter measurement; Cary 50 spectrophotometer (Varian, Palo Alto, CA, USA) for ultraviolet (UV)–visible absorption spectra measurement; F-182 4500 spectrophotometer (Hitachi) for fluorescence measurement; and RBD-upgraded PHI-5000C ESCA system (Perkin Elmer, Waltham, MA, USA) for X-ray photoelectron spectroscopy (XPS).

Preparation of NCs

Gd–Au NCs were synthesized using an improved "facile" synthetic route reported previously.[28] Briefly, 250 mg BSA and 5 mL water were mixed. Then, 5 mL $HAuCl_4$ solution (10 mM) was slowly added to the mixture. Ten minutes later, 0.15 mL $GdCl_3$ solution (500 mM) was slowly added to the mixture with stirring; 0.75 mL 1 M NaOH was then added 10 minutes later, and the solution was stirred at 37°C for 12 hours. The Gd–Au NCs were purified using dialysis and then freeze-dried. They were then dissolved with appropriate media on the day of use.

GPC-1 antibody (Abcam, Cambridge, UK) was conjugated with Gd–Au NCs by EDC.[29] Briefly, 30 mg Gd–Au NCs were dissolved in 900 µL PBS, and 10 mg EDC was dissolved in 100 µL PBS. After adding EDC solution (100 µL) to Gd–Au NC solution (900 µL), the solution was mixed for 5 minutes at room temperature (RT) with sonication. GPC-1 antibody (30 µL) was then added into the activated Gd–Au NC solution at RT for 2 hours with stirring, protected from light. The mixture underwent centrifugal ultrafiltration (4,000 rpm, 20 minutes) and was washed with PBS 3 times, and the conjugates were then diluted with PBS (hereafter referred to as Gd-Au-NC-GPC-1).

Cell culture and in vitro cytotoxicity

Human PC cells (COLO-357) and human normal cell lines (293T) were used in this study. COLO-357 cells were obtained from the Second Military Medical University

(Shanghai, China). 293T cells were obtained from Tongji University School of Medicine (Shanghai, China). All cells were maintained according to the previously described methods and were cultured at 37°C in a 5% CO_2 incubator. This research was approved by the Second Military Medical University Institutional Review Board (Shanghai, China).

For in vitro cytotoxicity testing, COLO-357 or 293T (8×10^3 cells/well) cells were cultured in 96-well plates at 37°C in the presence of 5% CO_2. The next day, Cell Counting Kit-8 (CCK-8) assays were performed following the manufacturer's protocol (ZOMANBIO, Beijing, China). Briefly, cultured media were removed and replaced with 200 µL fresh culture media containing Gd–Au NCs or Gd-Au-NC-GPC-1 in various concentrations. The mixture of target cells and NCs was incubated at 37°C for 24 hours. Then, the media were removed, and the cells were washed 2 times with PBS and were then incubated in fresh media with CCK-8 solution at 37°C for 1 hour. Absorbance at 450 nm was measured using an enzyme-linked immunosorbent assay (ELISA) Plate Reader (Thermo Fisher Scientific, Waltham, MA, USA). Three independent biological experiments were performed.

Fluorescence labeling in vitro

COLO-357 and 293T cells were seeded in culture dishes at a seeding density of 2×10^5 cells/well and incubated for 24 hours under culture conditions. After incubation, the cells were washed 2 times with PBS and then treated with Gd-Au-NC-GPC-1 or Gd–Au NCs at Au concentration of 0.46 mM for 2 hours. After discarding NCs, the cells were washed 2 times with PBS and then visualized using a Leica confocal microscope (Leica TCS SP5 II, Wetzlar, Germany) with a 60× oil objective. The cells were then digested with Trypsin (Hyclone, Logan, UT, USA), washed 2 times with PBS, and resuspended in 0.5 mL PBS. The fluorescence intensity analysis was performed by flow cytometry using a BD FACSVerse and FlowJo_V10 cytometers (BD Bioscience, Lake Franklin, NJ, USA). We gated the fluorescence intensities from cells incubated without NCs as baseline fluorescence. We then analyzed and compared the percentages of cells with positive fluorescence in the different groups. Three independent experiments were performed.

Relaxometry and in vitro MRI

The longitudinal (T1) and transverse (T2) relaxation times of Gd-Au-NC-GPC-1 were evaluated by using a 1.41 T minispec mq60 NMR Analyzer (Bruker Optik GmbH, Ettlingen, Germany) at 37°C. Relaxivity values of r1 and r2 were calculated by fitting the 1/T1 and 1/T2 relaxation time (s^{-1}) versus the Gd concentration (mM) curves.

For in vitro MRI, COLO-357 and 293T cells (2×10^6) were treated with various concentrations of Gd-Au-NC-GPC-1 at 37°C for 2 hours. The cells were then washed 3 times with PBS and harvested by trypsinization for 3 minutes. After centrifugation at 1,000 rpm for 5 minutes, the cells were resuspended in 20 µL PBS in an Eppendorf Tube® (Axygen, CA, USA). Magnetic resonance images were acquired using a 3.0 T MAGNETOM Skyra MRI scanner (Siemens, Erlangen, Germany) using T1-weighted sequence (Mapping, repetition time/echo time [TR/TE] =6.83/2.26 ms, thickness =2 mm).

Animal model and immunohistochemical (IHC) staining

Male nude mice (4–5 weeks old) were purchased from Shanghai Laboratory Animal Center of the Chinese Academy of Sciences (Shanghai, China). To develop the mouse tumor model, 1×10^6 COLO-357 cells were subcutaneously injected into the axillary fossa of each mouse. Experiments were performed on COLO-357 tumor-bearing mice when tumor volumes reached about 60 mm^3. All mouse experiments were approved by and performed according to the guidelines of the Second Military Medical University Laboratory Animal Center (Shanghai, China; approval ID: #20170105024).

IHC staining was performed as previously described using the GPC-1 antibody.[30] Integrated optical density (IOD) was analyzed using Image-pro plus 6.0 (Media Cybernetics Inc., Rockville, MD, USA).

In vivo FI/MRI

For in vivo FI, 200 µL Gd–Au NCs or Gd-Au-NC-GPC-1 (Au: 37 µM/kg) was intravenously injected into each COLO-357 tumor-bearing mouse (n=3). Then, fluorescence images were acquired at different time points before (0 minute) and after (10, 30, and 40 minutes) tail vein injection. FI was performed using an IVIS Lumina II (Hopkinton, MA, USA). The excitation wavelength of filter was 535 nm, and the emission wavelength was 670 nm. In addition, relative fluorescence intensity of the tumor region was measured and expressed as mean ± SD.

For in vivo MRI, 200 µL Gd–Au NCs or Gd-Au-NC-GPC-1 (Gd: 50 µM/kg) was intravenously injected into each COLO-357 tumor-bearing mouse (n=3). Then, MR images were obtained at different time points before (0 minute) and after (10, 30, 60, and 120 minutes) tail vein injection. MRI was performed using a 3.0 T MAGNETOM Skyra MRI scanner (Siemens) using T1-weighted sequence (Mapping, TR/TE =6.83/2.26 ms, thickness =2 mm). In addition, the relative MR intensity of the tumor region was measured and expressed as mean ± SD.

In vivo toxicity of NCs

To evaluate the acute toxicological effects of Gd-Au-NC-GPC-1 in vivo, healthy nude mice (n=3) were intravenously injected with 200 μL saline solution or Gd-Au-NC-GPC-1 (Gd: 50 μM/kg). Mice injected with saline solution were used as the control. All nude mice were anaesthetized and euthanized 24 hours later. For blood chemistry analysis, serum biochemistry analysis was performed using an Automatic Chemistry Analyzer Chemray 240 (Rayto Life and Analytical Sciences Co., Ltd., Shenzhen, China). For histology examinations, appropriate organs were harvested and stained with hematoxylin and eosin (H&E). Pathological changes were observed using an optical microscope.

Results and discussion

Preparation and characterization of Gd-Au-NC-GPC-1

Gd–Au NCs were prepared according to the methods previously reported by our group.[28] BSA, commonly employed as a substrate for biomineralization, was selected as the model protein for this study. Upon adding $HAuCl_4$ and $GdCl_3$ to the aqueous BSA solution, the protein molecules sequestered and entrapped Au and Gd ions.[31,32]

GPC-1 antibody was then conjugated with Gd–Au NCs using EDC, a water-soluble carbodiimide crosslinker.[29,33–35] Under these conjugation conditions, BSA was activated by EDC and then conjugated with GPC-1 antibody.[29]

HRTEM images showed a round-like morphology for Gd-Au-NC-GPC-1 with ~3 nm average diameter (Figure 1A), which was similar to the Gd–Au NCs (Figure S1A). Dynamic light scattering showed the hydrodynamic diameters of Gd-Au-NC-GPC-1 ranging from 13.5 to 24.4 nm with an average of 18.2 nm (Figure 1B), which was slightly larger than that of Gd–Au NCs (8.7 nm) due to GPC-1 antibody conjugation (Figure S1B). AFM 3-dimensional topographic images and line profiles showed a low surface roughness for Gd-Au-NC-GPC-1 (Figure 1C and D), which was similar to Gd–Au NCs (Figure S1C and D). From the data obtained from 3-dimensional topographic images and line profiles by AFM, we conclude the following: 1) the surface roughness of both nanomaterials (Gd-Au-NC-GPC-1 and Gd–Au NCs) were low; 2) the height distributions of both nanomaterial surfaces were homogeneous; 3) the average thickness of Gd-Au-NC-GPC-1 (23 nm) was slightly greater than that of Gd–Au NCs (18 nm) due to GPC-1 antibody conjugation; and 4) the thickness of both nanomaterials demonstrates the frame role that BSA plays in the 2 nanomaterials. The chemical structures of the probes were characterized using XPS. The C1s XPS spectra showed that 6 components are found to be associated with carbon atoms in the C1s region: O–C=O (289.1 eV), C=O (287.7 eV), C–O (286.5 eV), C–N (285.7 eV), C–C (284.5 eV), and C=C (283.2 eV). For Gd-Au-NC-GPC-1, the intensity peak of O–C=O was missing, indicating that the conjugation between carboxyl groups and primary amines was successful. The intensity peak of C=C in Gd-Au-Nc-GPC-1, which mostly came from the GPC-1 antibody, indicated successful conjugation of the GPC-1 antibody to Gd–Au NCs (Figure 1E and F).

Property characterization of Gd-Au-NC-GPC-1

Property characterization of Gd-Au-NC-GPC-1 indicated that there was no significant influence by conjugating the GPC-1 antibody. As shown in Figure 2A, Gd-Au-NC-GPC-1 had absorption at 280 nm. The absorption peak was less well defined in Gd-Au-NC-GPC-1 compared with Gd–Au NCs (Figure S2A), which was mostly associated with ultrafiltration. It has been reported that the absorption peak at 280 nm originates from the aromatic amino acid.[36] As free BSA was removed during purification by ultrafiltration, the absorption peak in the Gd-Au-NC-GPC-1 became less well defined. Fluorescence emission spectra showed that strong fluorescence at 650 nm was observed from Gd-Au-NC-GPC-1 (Figure 2B), which was similar to that of Gd–Au NCs (Figure S2B). Using a 365-nm UV-lamp irradiation, Gd-Au-NC-GPC-1 exhibits strong fluorescence intensity as for Gd–Au NCs (Figures 2C and S2C), which make it an ideal FI contrast agent.

To evaluate the potential application of Gd-Au-NC-GPC-1 as an MRI contrast agent, the T1 and T2 relaxivity values were measured at different Gd concentrations. As shown in Figure 2D, the r1 value of Gd-Au-NC-GPC-1 was 17.722 s^{-1} mM^{-1} Gd, which was almost 4 times higher compared with the r1 value of Gd-diethylenetriaminepentacetate (DTPA; a clinical MRI contrast agent; r1 value =4.6 s^{-1} mM^{-1} Gd).[36] In addition, the ratio of r2 to r1 was relatively low (r2/r1 =1.39, r2/r1$<$3), indicating a strong T1 effect.[37] In this study, we considered 3 as a useful cutoff r2/r1 ratio, because most of the T1 contrast agents had r2/r1 ratios ranging between 1 and 2, while the r2/r1 ratios for T2 contrast agents are always much higher (iron oxide particles $\geq$10).[37,38] Next, the T1-weighted MR images were compared (Figures 2E and S2D). Gd-Au-NC-GPC-1 exhibits similar MR signals as Gd-DTPA even at lower Gd concentrations (Figure 2E). Results showed that MR signals between Gd-Au-NC-GPC-1 and Gd–Au NCs were almost same, which indicated that

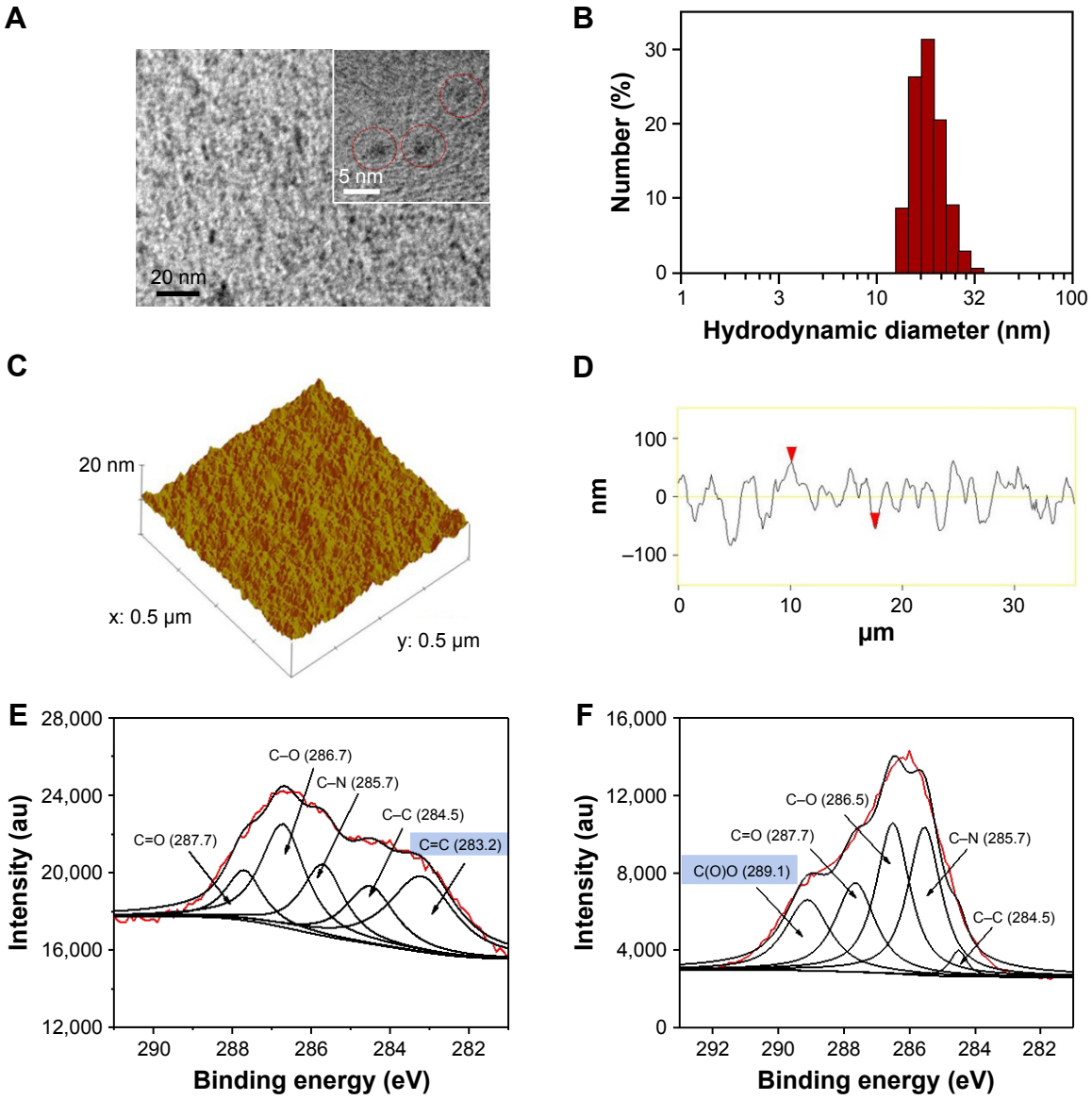

Figure 1 (**A**) TEM image of Gd-Au-NC-GPC-1 (red circles). (**B**) Hydrodynamic diameter distribution of Gd-Au-NC-GPC-1. (**C**) Topographic profile of Gd-Au-NC-GPC-1. (**D**) Line profile of Gd-Au-NC-GPC-1. (**E**) The C1s XPS spectra of Gd-Au-NC-GPC-1. (**F**) The C1s XPS spectra of Gd–Au NCs.
Note: (**D**) Red arrowheads: two points selected artificially during the process of cartography, in order to determine the location of the line profile.
Abbreviations: Gd-Au-NC-GPC-1, Gd–Au NCs conjugated with GPC-1 antibody; GPC-1, Glypican-1; NCs, nanoclusters; TEM, transmission electron microscopy; XPS, X-ray photoelectron spectroscopy.

the conjugation of the GPC-1 antibody did not result in significant influence on MR signals from Gd–Au NCs. These results suggest that Gd-Au-NC-GPC-1 could be used as a T1-positive contrast agent.

Cell toxicity of Gd-Au-NC-GPC-1

In order to test the cell toxicity of Gd-Au-NC-GPC-1, we selected human PC cells (COLO-357) and human normal cell lines (293T) as our target cells. CCK-8 assays were used to determine cell toxicity.[33] The results of target cells treated with both Gd–Au NCs and Gd-Au-NC-GPC-1 at various concentrations for 24 hours are shown in Figure 3. Concentrations ranging from 0 to 150 mg/L were tested. Results indicated that there was no significant cytotoxicity (cell viability >80%) for Gd–Au NCs against both COLO-357 (Figure 3A) and 293T cells (Figure 3B) at all the concentrations tested, which was consistent with our previously published results.[28] For Gd-Au-NC-GPC-1, no significant cytotoxicity was observed in 293T cells at all concentrations tested, which was similar to Gd–Au NCs (Figure 3B). However, Gd-Au-NC-GPC-1 showed dose-dependent cytotoxicity (cell viability: from 75.7% to 37.4%) against COLO-357 cells at relatively high concentrations (concentrations: from 30 to 150 mg/L; Figure 3A), which may be associated with

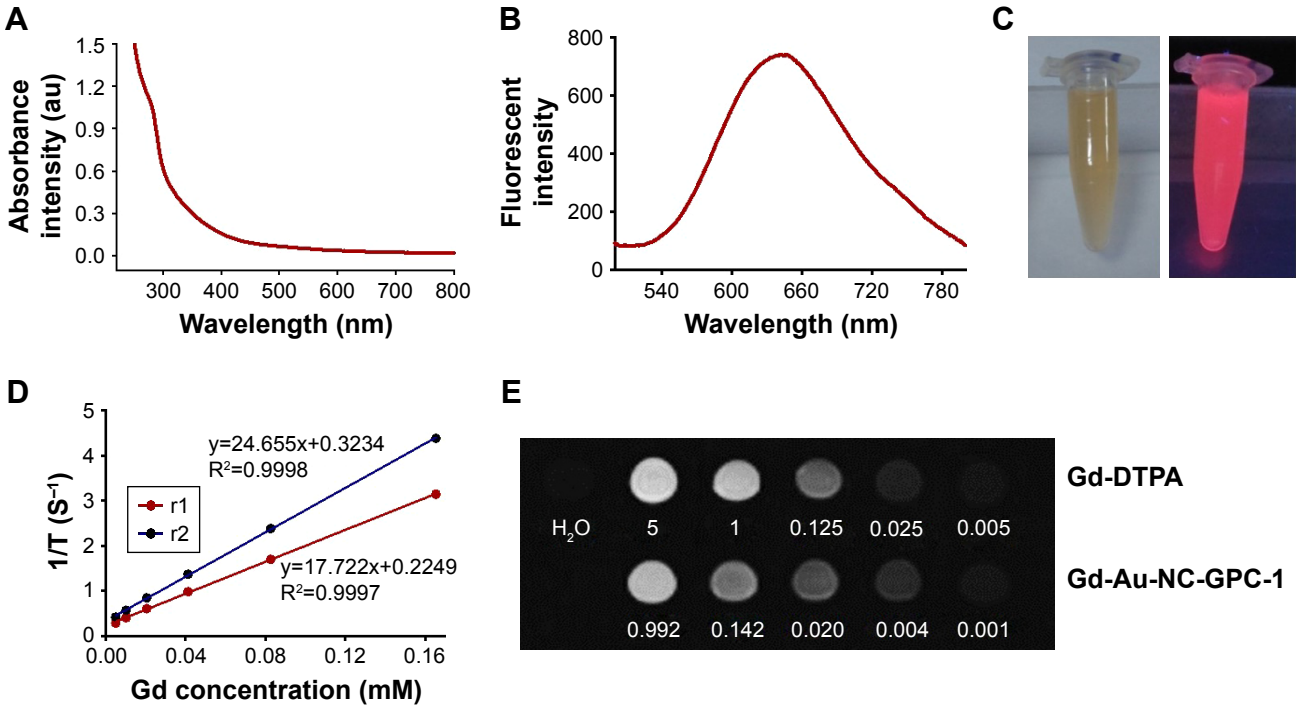

Figure 2 (**A**) UV–visible absorption spectra of Gd-Au-NC-GPC-1. (**B**) Fluorescent emission spectra of Gd-Au-NC-GPC-1. (**C**) Bright (left) and fluorescent (right) photograph of Gd-Au-NC-GPC-1. (**D**) T1 and T2 relaxation times of Gd-Au-NC-GPC-1. (**E**) T1-weighted MR images of Gd-DTPA and Gd-Au-NC-GPC-1 at various concentrations (mM).

Abbreviations: DTPA, diethylenetriaminepentacetate; Gd-Au-NC-GPC-1, Gd–Au NCs conjugated with GPC-1 antibody; GPC-1, Glypican-1; MR, magnetic resonance; NCs, nanoclusters; UV, ultraviolet.

complement-dependent cytotoxicity.[39] Gd-Au-NC-GPC-1 showed selective cell toxicity to PC cells, but almost no toxicity to human normal cells (293T cells), indicating that Gd-Au-NC-GPC-1 would be a promising agent for in vivo use.

Dual-modal imaging of PC cells in vitro

As Gd-Au-NC-GPC-1 exhibits strong fluorescence at 650 nm, it is possible to detect PC cells by FI using confocal microscopy and flow cytometry. COLO-357 and 293T cells were incubated with Gd-Au-NC-GPC-1 or Gd–Au NCs (Au concentration: 0.46 mM) at 37°C for 2 hours (Figure 4A). Gd-Au-NC-GPC-1 exhibits strong red fluorescence on the surface of COLO-357 cells, but was rather weak on the surface of 293T cells. In contrast, incubating with Gd–Au NCs, the red fluorescence on the surface of both COLO-357 and 293T cells was almost absent. These results suggest that Gd-Au-NC-GPC-1 is a selective FI agent for detecting PC cells in vitro. Next, we investigated whether the labeling of PC cells

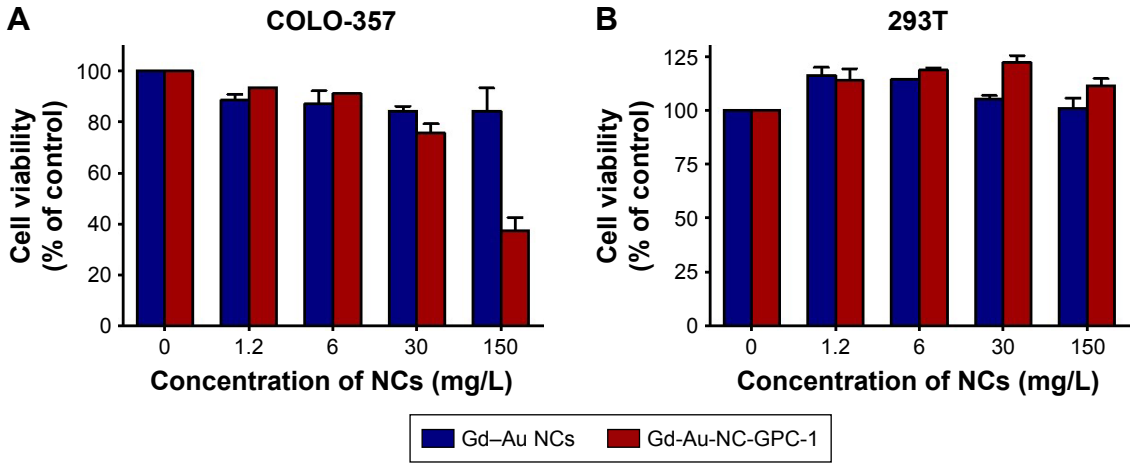

Figure 3 Cell viability of COLO-357 (**A**) and 293T cells (**B**) after incubation with different concentrations of Gd–Au NCs (blue) or Gd-Au-NC-GPC-1 (red) for 24 hours.

Abbreviations: Gd-Au-NC-GPC-1, Gd–Au NCs conjugated with GPC-1 antibody; GPC-1, Glypican-1; NCs, nanoclusters.

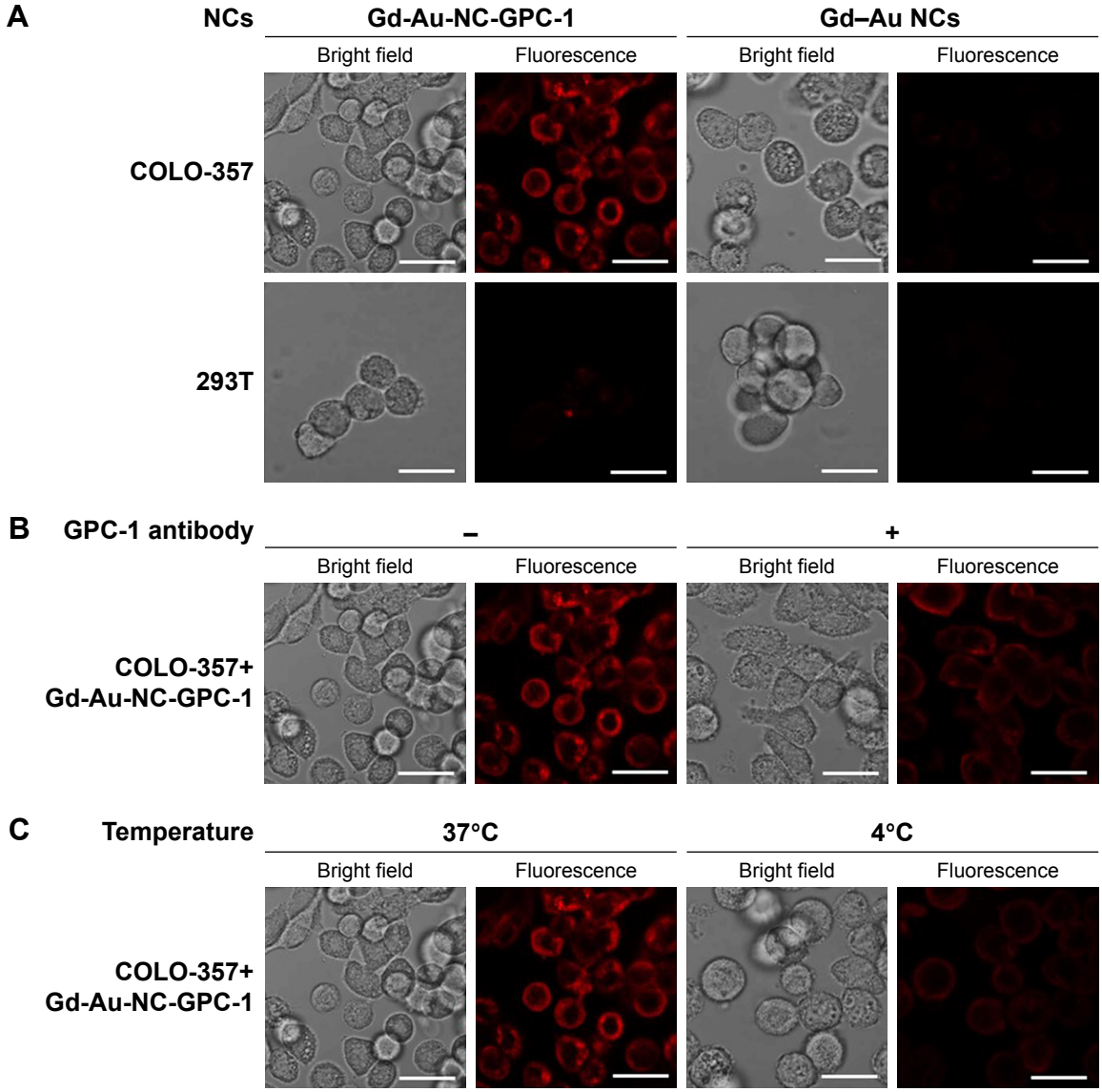

Figure 4 Confocal fluorescence images of in vitro cell uptake of Gd-Au-NC-GPC-1 at Au concentration of 0.46 mM. (**A**) COLO-357 and 293T cells were incubated with Gd-Au-NC-GPC-1 or Gd–Au NCs at 37°C for 2 hours. (**B**) COLO-357 cells were preincubated with or without GPC-1 antibody (dilution rate, 1:50) at 37°C for 2 hours. After discarding GPC-1 antibody and washing target cells with PBS 2 times, COLO-357 cells were incubated with Gd-Au-NC-GPC-1 at 37°C for another 2 hours. (**C**) COLO-357 cells were incubated with Gd-Au-NC-GPC-1 at 37°C or 4°C for 2 hours. Bar, 25 μm.
Abbreviations: Gd-Au-NC-GPC-1, Gd–Au NCs conjugated with GPC-1 antibody; GPC-1, Glypican-1; NCs, nanoclusters.

by Gd-Au-NC-GPC-1 is through specific binding of GPC-1 antibody to antigen. We preincubated COLO-357 cells with GPC-1 antibody at 37°C for 2 hours, followed by incubation with Gd-Au-NC-GPC-1 at 37°C for another 2 hours (Figure 4B). If Gd-Au-NC-GPC-1 labeling of PC cells was through the specific binding of GPC-1 antibody to antigen, then GPC-1 antibody will competitively bind to GPC-1 antigen in the preincubation stage, leading to reduced binding of Gd-Au-NC-GPC-1 to PC cells. In addition, we incubated COLO-357 cells with Gd-Au-NC-GPC-1 at 4°C for 2 hours (Figure 4C). It is known that the optimal condition for most IgG antibody binding to antigen is at 37°C; hence, the low temperature would reduce the binding rate of antibody and antigen.[40] If Gd-Au-NC-GPC-1 labeling of PC cells was through the specific binding of GPC-1 antibody to antigen, the incubation temperature at 4°C will reduce the binding rate of Gd-Au-NC-GPC-1 to PC cells. Results showed that the intensity of fluorescence was reduced for both GPC-1 antibody preincubation and 4°C incubation. These results suggest that the FI of PC cells by Gd-Au-NC-GPC-1 was through specific binding of GPC-1 antibody to antigen.

As shown in Figure 5A, the fluorescence intensity values of Gd–Au NCs on COLO-357 and 293T cells were quite low (COLO-357: 0.42%; 293T: 0.23%). In sharp contrast, the fluorescence intensity of Gd-Au-NC-GPC-1 on COLO-357 cells was enhanced significantly (99.4%). However, the

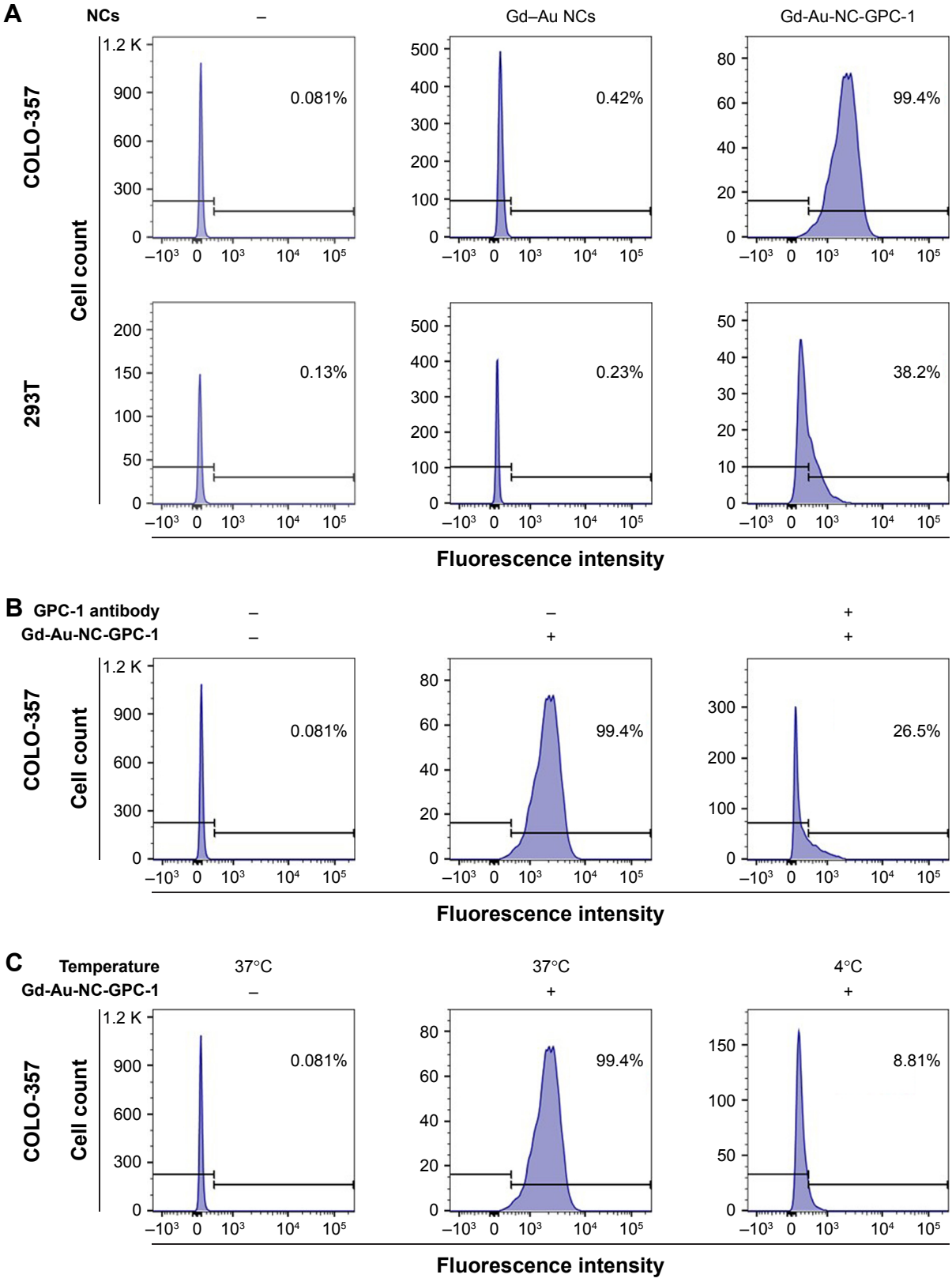

Figure 5 GPC-1 targeted uptake analysis of Gd-Au-NC-GPC-1 at Au concentration of 0.46 mM by flow cytometry. (**A**) COLO-357 and 293T cells were incubated with Gd-Au-NC-GPC-1 or Gd–Au NCs at 37°C for 2 hours. (**B**) COLO-357 cells were preincubated with or without GPC-1 antibody (dilution rate, 1:50) at 37°C for 2 hours. After discarding GPC-1 antibody and washing target cells with PBS 2 times, COLO-357 cells were incubated with Gd-Au-NC-GPC-1 at 37°C for another 2 hours. (**C**) COLO-357 cells were incubated with Gd-Au-NC-GPC-1 at 37°C or 4°C for 2 hours.

Abbreviations: Gd-Au-NC-GPC-1, Gd–Au NCs conjugated with GPC-1 antibody; GPC-1, Glypican-1; NCs, nanoclusters.

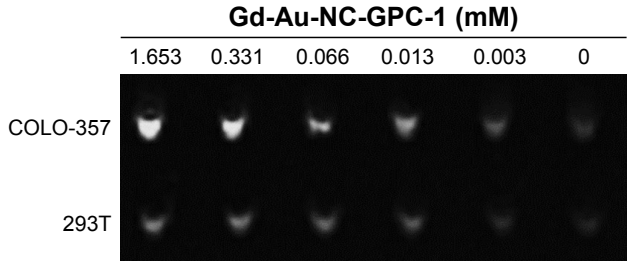

Figure 6 In vitro MRI study with COLO-357 and 293T cells.
Abbreviations: Gd-Au-NC-GPC-1, Gd–Au NCs conjugated with GPC-1 antibody; GPC-1, Glypican-1; MRI, magnetic resonance imaging; NCs, nanoclusters.

fluorescence intensity of Gd-Au-NC-GPC-1 on 293T cells was slightly enhanced (38.2%). These data indicate that Gd-Au-NC-GPC-1 was a selective FI agent for labeling PC cells in vitro, which is consistent with the results obtained by confocal microscopy. Figure 5B shows that preincubation with GPC-1 antibody reduced the fluorescence intensity of Gd-Au-NC-GPC-1 on COLO-357 cells (26.5%). Figure 5C shows that incubation at 4°C also reduced the fluorescence intensity of Gd-Au-NC-GPC-1 on PC cells (8.81%). These data suggest that the fluorescence labeling of Gd-Au-NC-GPC-1 is through specific binding of GPC-1 antibody to antigen, which is consistent with the results obtained by confocal microscopy. These results indicate that Gd-Au-NC-GPC-1 is a potential FI contrast agent with a strong in vitro GPC-1 targeting capability.

Since Gd-Au-NC-GPC-1 exhibits a strong T1 effect, it is possible to detect PC cells by MRI. Figure 6 shows the MR signal intensities of COLO-357 and 293T cells treated with various concentrations of Gd-Au-NC-GPC-1. Data show that the cells treated with Gd-Au-NC-GPC-1 exhibit concentration-dependent MR signal intensity. In addition, MR signal intensity of COLO-357 cells was much stronger compared with 293T cells, which was associated with the strong GPC-1 targeting capability of Gd-Au-NC-GPC-1. These results suggest that Gd-Au-NC-GPC-1 is a promising selective positive MRI contrast agent for detecting PC cells in vitro.

Dual-modal imaging of PC cells in vivo

We next investigated the dual-modal imaging effect of Gd-Au-NC-GPC-1 in vivo. COLO-357 tumor-bearing nude mice were used as animal models. To investigate the level of GPC-1 in the tumor tissues of COLO-357 tumor-bearing nude mice, we performed IHC staining of GPC-1 in COLO-357 tumor tissues and adjacent normal tissues (Figure 7A and B). The results of IOD analysis showed that the expression level of GPC-1 in COLO-357 tumor tissues was significantly higher than that of normal tissues (Figure 7C), which was consistent with the previous reports.[12]

After intravenous injection with 200 µL Gd–Au NCs or Gd-Au-NC-GPC-1 into tumor-bearing mice, in vivo fluorescence images and MR images were obtained at different

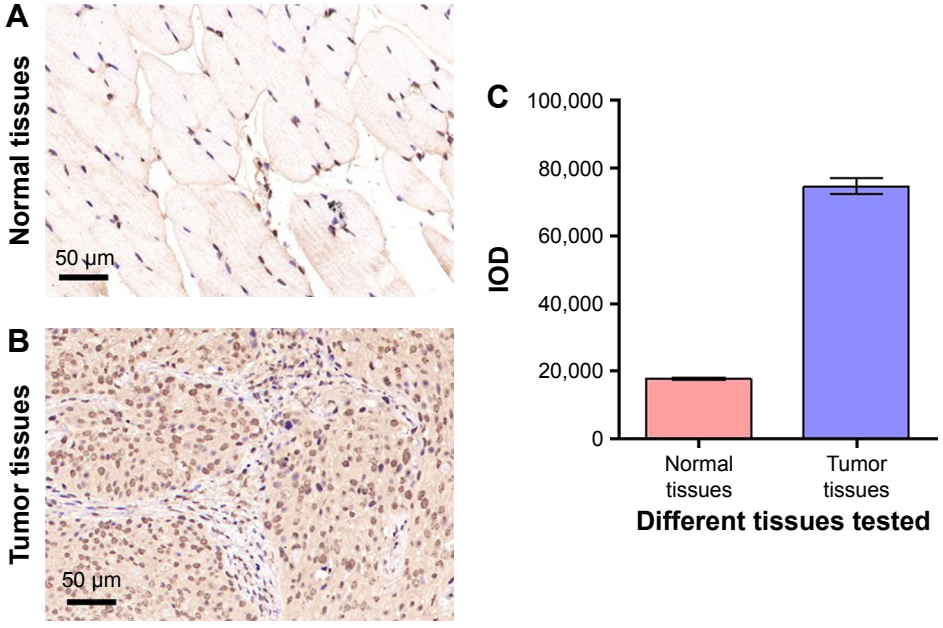

Figure 7 GPC-1 is increased in the tumor tissues of COLO-357 tumor-bearing nude mice. (**A**, **B**) IHC staining of GPC-1 (brown color) in the normal tissues (**A**) and COLO-357 tumor tissues (**B**). (**C**) IOD of the results of (**A**, **B**).
Abbreviations: GPC-1, Glypican-1; IHC, immunohistochemical; IOD, integrated optical density.

time points. Figure 8A shows the fluorescence images of NCs in vivo. Figure 8B shows the relative fluorescence intensities of tumor sites. For Gd–Au NCs-treated mice, the fluorescent intensities in tumor sites gradually increased during the first 10 minutes after injection and decreased slightly during the following 30 minutes. We inferred that the enhancement of fluorescence signal may be attributable to the enhanced permeability and retention (EPR) effect.[36] For Gd-Au-NC-GPC-1-treated mice, the fluorescence intensity in tumor sites increased with time, reached a peak at 30 minutes after injection, and then subsequently decreased during the next 10 minutes. The fluorescence signal of tumor sites in the Gd-Au-NC-GPC-1 group was much higher than that in the Gd–Au NCs group, suggesting the strong GPC-1 targeting capacity of Gd-Au-NC-GPC-1 in vivo. Although the results of FI had limited spatial resolution, the high detection sensitivity makes Gd-Au-NC-GPC-1 an ideal FI contrast agent for detecting PC cells.

Figure 8C shows the MR images of NCs in vivo. In addition, Figure 8D shows the relative MR intensities of tumor sites. For Gd–Au NCs-treated mice, the MR signal in the tumor site increased gradually during the first 60 minutes and then started to decrease during the next 60 minutes. Similarly, we inferred that the time-dependent increase of MR signal in the Gd–Au NCs group was also associated with the EPR effect.[36] For Gd-Au-NC-GPC-1-treated mice, an obviously bright MR signal was observed in the tumor site at 30 minutes after injection. The MR signal in the Gd-Au-NC-GPC-1-treated group was earlier and stronger than that in the Gd–Au NCs-treated group. These results confirmed the strong GPC-1 targeting

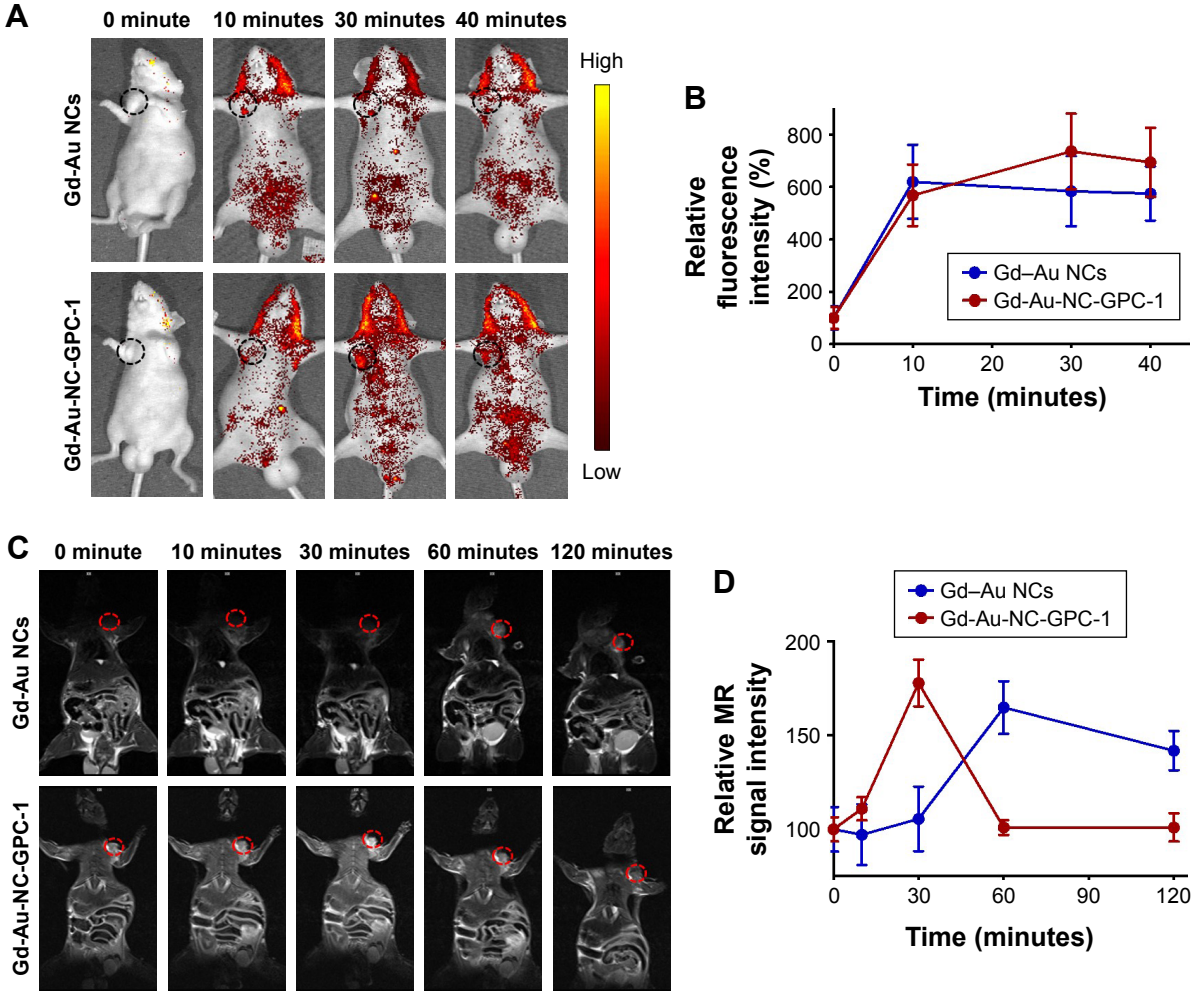

Figure 8 In vivo FI and MRI of COLO-357 tumor-bearing nude mice in the supine position. (**A**) Fluorescence images were taken at different time points after intravenous injection of Gd–Au NCs or Gd-Au-NC-GPC-1. The tumor sites are marked by black dotted circles. (**B**) Relative fluorescence intensities of tumor sites relate to (**A**). (**C**) T1-weighted MR images were taken at different time points after intravenous injection of Gd–Au NCs or Gd-Au-NC-GPC-1. The tumor sites are marked by red dotted circles. (**D**) Relative MR signal intensities of tumor sites relate to (**C**).

Abbreviations: FI, fluorescence imaging; Gd-Au-NC-GPC-1, Gd–Au NCs conjugated with GPC-1 antibody; GPC-1, Glypican-1; MRI, magnetic resonance imaging; NCs, nanoclusters.

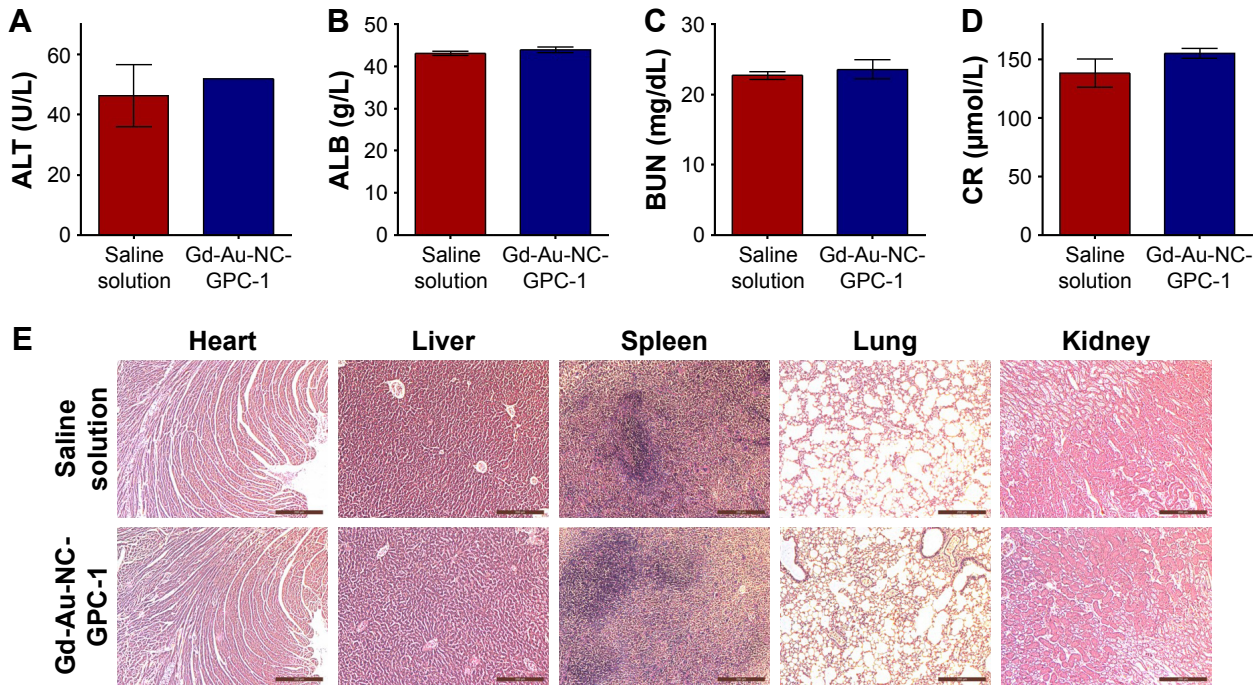

Figure 9 Acute toxicology evaluation of Gd-Au-NC-GPC-1 in vivo. Healthy nude mice were intravenously injected with 200 μL saline solution or Gd-Au-NC-GPC-1 (Gd: 50 μM/kg) and then were euthanized 24 hours later (n=3). (**A**–**D**) Results of serum biochemistry analysis. (**E**) H&E stained images of mice visceral organs. Scale bar: 200 μm.
Abbreviations: ALB, albumin; ALT, alanine aminotransferase; BUN, blood urea nitrogen; CR, creatinine; Gd-Au-NC-GPC-1, Gd–Au NCs conjugated with GPC-1 antibody; GPC-1, Glypican-1; H&E, hematoxylin and eosin; NCs, nanoclusters.

capacity of Gd-Au-NC-GPC-1 in vivo, which was consistent with the results of FI. Although the results of MRI had low sensitivity, the high spatial resolution makes Gd-Au-NC-GPC-1 an ideal MRI contrast agent for detecting PC cells.

It is documented that FI has high detection sensitivity, but suffers from limited spatial resolution.[23,24] Conversely, MRI has high anatomical resolution, but lacks the sensitivity.[25–27] The sensitivity of Gd-Au-NC-GPC-1 with dual-modal FI/MRI function is reflected in the following aspects: 1) in the dual-modal imaging of PC cells in vitro, MRI could only demonstrate whether or how much Gd-Au-NC-GPC-1 was located with PC cells or the combination degree. However, FI could clearly show that Gd-Au-NC-GPC-1 was targeted on the cell membrane of COLO-357 cells; and 2) in the dual-modal imaging of PC cells in vivo, FI could only demonstrate whether Gd-Au-NC-GPC-1 was targeted to the tumor and the approximate position of the tumor in the mouse. However, MRI could clearly show the exact location of the tumor based on the position of other organs. In this study, Gd-Au-NC-GPC-1 not only demonstrated the targeting spot at the cellular level, but also showed the exact location of the tumor in vivo. Therefore, Gd-Au-NC-GPC-1 with dual-modal FI/MRI function has the potential to be used both for the early diagnosis of PC in the clinic and as a research tool to determine the mechanism of action at the cellular level.

In vivo toxicity of Gd-Au-NC-GPC-1

To investigate the acute toxicity of Gd-Au-NC-GPC-1 in vivo, serum biochemistry and histological examinations were performed (Figure 9). Healthy nude mice (n=3) were intravenously injected with 200 μL saline solution or Gd-Au-NC-GPC-1 (Gd: 50 μM/kg) and then euthanized 24 hours later. The results of serum biochemistry analysis showed that there were no significant differences between the saline solution and Gd-Au-NC-GPC-1 group. Both liver function markers (Figure 9A and B) and kidney function markers (Figure 9C and D) in the Gd-Au-NC-GPC-1 group were within the normal range. H&E staining images of 5 major organs (heart, liver, spleen, lung, and kidney) from the saline-solution-injected mice and Gd-Au-NC-GPC-1-injected mice were compared (Figure 9E). Compared with the saline-solution-injected mice, there were no obvious pathology changes in the major organs of the Gd-Au-NC-GPC-1-injected mice. These results indicate that Gd-Au-NC-GPC-1 has good biosafety at the tested dose, which makes possible further clinical application.

Conclusion

We established a new multifunctional nanoprobe designated Gd-Au-NC-GPC-1 for detecting PC cells. Dual-modal Gd-Au-NC-GPC-1 nanoprobe exhibits intense red fluorescent

emission and strong T1 effect. Conjugation with GPC-1 antibody enabled the functional imaging probe to effectively target GPC-1-expressing PC cells both in vitro and in vivo. Gd-Au-NC-GPC-1 could be a promising candidate for detecting PC cells in the clinic.

Acknowledgments

This study was supported by the Natural Science Foundation of China (Numbers: 81772285 and 31671029), Shanghai Health and Family Planning Commission Project (Number: 2017YQ051), Shanghai Science and Technology Commission Project (Number: 17411968700), and Shanghai Natural Science Foundation (Number: 16ZR1400700).

Author contributions

All authors contributed toward data analysis, drafting and revising the paper and agree to be accountable for all aspects of the work.

Disclosure

The authors report no conflicts of interest in this work.

References

1. Kamisawa T, Wood LD, Itoi T, Takaori K. Pancreatic cancer. *Lancet*. 2016;388(10039):73–85.
2. Wolfgang CL, Herman JM, Laheru DA, et al. Recent progress in pancreatic cancer. *CA Cancer J Clin*. 2013;63(5):318–348.
3. Gillen S, Schuster T, Meyer Zum Buschenfelde C, Friess H, Kleeff J. Preoperative/neoadjuvant therapy in pancreatic cancer: a systematic review and meta-analysis of response and resection percentages. *PLoS Med*. 2010;7(4):e1000267.
4. Kaur S, Baine MJ, Jain M, Sasson AR, Batra SK. Early diagnosis of pancreatic cancer: challenges and new developments. *Biomark Med*. 2012;6(5):597–612.
5. Zhou B, Xu JW, Cheng YG, et al. Early detection of pancreatic cancer: where are we now and where are we going? *Int J Cancer*. 2017; 141(2):231–241.
6. Wong KK, Qian Z, Le Y. The role of precision medicine in pancreatic cancer: challenges for targeted therapy, immune modulating treatment, early detection, and less invasive operations. *Cancer Transl Med*. 2016;2(2):41–47.
7. Hussain SP. Pancreatic cancer: current progress and future challenges. *Int J Biol Sci*. 2016;12(3):270–272.
8. Jazieh KA, Foote MB, Diaz LA Jr. The clinical utility of biomarkers in the management of pancreatic adenocarcinoma. *Semin Radiat Oncol*. 2014;24(2):67–76.
9. Chan A, Prassas I, Dimitromanolakis A, et al. Validation of biomarkers that complement CA19.9 in detecting early pancreatic cancer. *Clin Cancer Res*. 2014;20(22):5787–5795.
10. Hanada K, Okazaki A, Hirano N, et al. Diagnostic strategies for early pancreatic cancer. *J Gastroenterol*. 2015;50(2):147–154.
11. Melo SA, Luecke LB, Kahlert C, et al. Glypican-1 identifies cancer exosomes and detects early pancreatic cancer. *Nature*. 2015;523(7559): 177–182.
12. Kleeff J, Ishiwata T, Kumbasar A, et al. The cell-surface heparan sulfate proteoglycan glypican-1 regulates growth factor action in pancreatic carcinoma cells and is overexpressed in human pancreatic cancer. *J Clin Invest*. 1998;102(9):1662–1673.
13. Duan L, Hu XQ, Feng DY, Lei SY, Hu GH. GPC-1 may serve as a predictor of perineural invasion and a prognosticator of survival in pancreatic cancer. *Asian J Surg*. 2013;36(1):7–12.
14. Weissleder R, Mahmood U. Molecular imaging. *Radiology*. 2001; 219(2):316–333.
15. Sangtani A, Nag OK, Field LD, Breger JC, Delehanty JB. Multifunctional nanoparticle composites: progress in the use of soft and hard nanoparticles for drug delivery and imaging. *Wiley Interdiscip Rev Nanomed Nanobiotechnol*. 2017;9(6).
16. Louie A. Multimodality imaging probes: design and challenges. *Chem Rev*. 2010;110(5):3146–3195.
17. Chen Q, Shang W, Zeng C, et al. Theranostic imaging of liver cancer using targeted optical/MRI dual-modal probes. *Oncotarget*. 2017; 8(20):32741–32751.
18. Dong A, Lan S, Huang J, et al. Modifying Fe3O4-functionalized nanoparticles with N-halamine and their magnetic/antibacterial properties. *ACS Appl Mater Interfaces*. 2011;3(11):4228–4235.
19. Yang J, Luo Y, Xu Y, et al. Conjugation of iron oxide nanoparticles with RGD-modified dendrimers for targeted tumor MR imaging. *ACS Appl Mater Interfaces*. 2015;7(9):5420–5428.
20. Guo W, Yang W, Wang Y, et al. Color tunable Gd-Zn-Cu-In-S/ZnS quantum dots for dual modality magnetic resonance and fluorescence imaging. *Nano Res*. 2014;7(11):1581–1591.
21. Yang W, Guo W, Gong X, et al. Facile synthesis of Gd-Cu-In-S/ZnS bimodal quantum dots with optimized properties for tumor targeted fluorescence/MR in vivo imaging. *ACS Appl Mater Interfaces*. 2015; 7(33):18759–18768.
22. Hu H, Huang P, Weiss OJ, et al. PET and NIR optical imaging using self-illuminating (64)Cu-doped chelator-free gold nanoclusters. *Biomaterials*. 2014;35(37):9868–9876.
23. Xu C, Wang Y, Zhang C, Jia Y, Luo Y, Gao X. AuGd integrated nanoprobes for optical/MRI/CT triple-modal in vivo tumor imaging. *Nanoscale*. 2017;9(13):4620–4628.
24. Zhang J, Hao G, Yao C, et al. Albumin-mediated biomineralization of paramagnetic NIR Ag2S QDs for tiny tumor bimodal targeted imaging in vivo. *ACS Appl Mater Interfaces*. 2016;8(26):16612–16621.
25. Xing X, Zhang B, Wang X, Liu F, Shi D, Cheng Y. An "imaging-biopsy" strategy for colorectal tumor reconfirmation by multipurpose paramagnetic quantum dots. *Biomaterials*. 2015;48:16–25.
26. Wang H, Zhou S. Magnetic and fluorescent carbon-based nanohybrids for multi-modal imaging and magnetic field/NIR light responsive drug carriers. *Biomater Sci*. 2016;4(7):1062–1073.
27. Bai J, Julie TW, Rubio N, et al. Triple-modal imaging of magnetically-targeted nanocapsules in solid tumours in vivo. *Theranostics*. 2016; 6(3):342–356.
28. Le W, Cui S, Chen X, Zhu H, Chen B, Cui Z. Facile synthesis of Gd-functionalized gold nanoclusters as potential MRI/CT contrast agents. *Nanomaterials (Basel)*. 2016;6(4):65.
29. Retnakumari A, Jayasimhan J, Chandran P, et al. CD33 monoclonal antibody conjugated Au cluster nano-bioprobe for targeted flow-cytometric detection of acute myeloid leukaemia. *Nanotechnology*. 2011;22(28):285102.
30. Ding H, Wei J, Zhao Y, Liu Y, Liu L, Cheng L. Progranulin derived engineered protein Atsttrin suppresses TNF-alpha-mediated inflammation in intervertebral disc degenerative disease. *Oncotarget*. 2017;8(65): 109692–109702.
31. Xie JP, Zheng YG, Ying JY. Protein-directed synthesis of highly fluorescent gold nanoclusters. *J Am Chem Soc*. 2009;131(3):888–889.
32. Isab AA, Hormann AL, Hill DT, Griswold DE, DiMartino MJ, Shaw CF. Bis(triethylphosphine)gold(I) chloride: ionization in aqueous solution, reduction in vitro of the external and internal disulfide bonds of bovine serum albumin and antiarthritic activity. *Inorg Chem*. 1989; 28(7):1321–1326.
33. Liu F, Le W, Mei T, et al. In vitro and in vivo targeting imaging of pancreatic cancer using a Fe3O4@SiO2 nanoprobe modified with anti-mesothelin antibody. *Int J Nanomedicine*. 2016;11:2195–2207.

34. Chou SW, Shau YH, Wu PC, Yang YS, Shieh DB, Chen CC. In vitro and in vivo studies of FePt nanoparticles for dual modal CT/MRI molecular imaging. *J Am Chem Soc*. 2010;132(38):13270–13278.
35. Retnakumari A, Setua S, Menon D, et al. Molecular-receptor-specific, non-toxic, near-infrared-emitting Au cluster-protein nanoconjugates for targeted cancer imaging. *Nanotechnology*. 2010;21(5):055103.
36. Sun SK, Dong LX, Cao Y, Sun HR, Yan XP. Fabrication of multi-functional Gd2O3/Au hybrid nanoprobe via a one-step approach for near-infrared fluorescence and magnetic resonance multimodal imaging in vivo. *Anal Chem*. 2013;85(17):8436–8441.
37. Caravan P, Ellison JJ, McMurry TJ, Lauffer RB. Gadolinium(III) chelates as MRI contrast agents: structure, dynamics, and applications. *Chem Rev*. 1999;99(9):2293–2352.
38. Kim BH, Lee N, Kim H, et al. Large-scale synthesis of uniform and extremely small-sized iron oxide nanoparticles for high-resolution T-1 magnetic resonance imaging contrast agents. *J Am Chem Soc*. 2011; 133(32):12624–12631.
39. Li H, Sun Y, Chen D, et al. Synergistic anti-tumor therapy by a comb-like multifunctional antibody nanoarray with exceptionally potent activity. *Sci Rep*. 2015;5:15712.
40. Armstrong B. Antigen–antibody reactions. *ISBT Sci Ser*. 2008;3(2): 21–32.

Supplementary materials

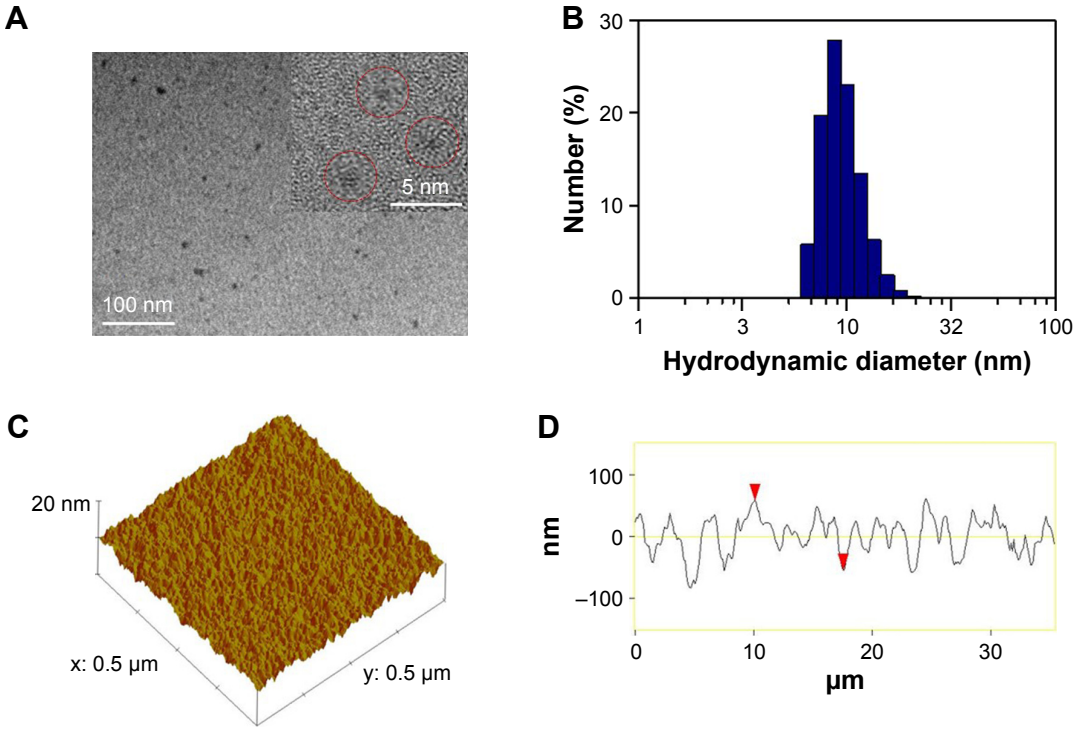

Figure S1 (**A**) TEM image of Gd–Au NCs. (**B**) Hydrodynamic diameter distribution of Gd–Au NCs. (**C**) Topographic profile of Gd–Au NCs. (**D**) Line profile of Gd–Au NCs.
Note: (**D**) Red arrowheads: two points selected artificially during the process of cartography, in order to determine the location of the line profile.
Abbreviations: Gd-Au-NC-GPC-1, Gd–Au NCs conjugated with GPC-1 antibody; GPC-1, Glypican-1; NCs, nanoclusters; TEM, transmission electron microscopy.

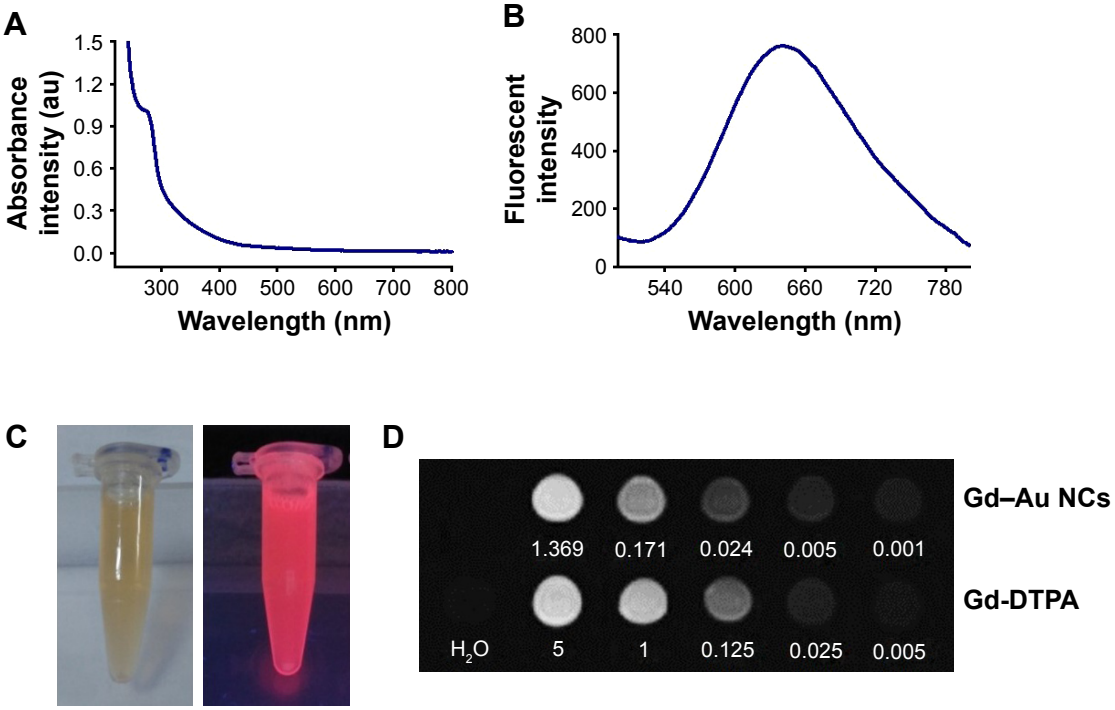

Figure S2 (**A**) UV–visible absorption spectra of Gd–Au NCs. (**B**) Fluorescent emission spectra of Gd–Au NCs. (**C**) Bright (left) and fluorescent (right) photograph of Gd–Au NCs. (**D**) T1-weighted MR images of Gd-DTPA and Gd–Au NCs with various concentrations (mM).
Abbreviations: DTPA, diethylenetriaminepentacetate; Gd-Au-NC-GPC-1, Gd–Au NCs conjugated with GPC-1 antibody; GPC-1, Glypican-1; MR, magnetic resonance; NCs, nanoclusters; UV, ultraviolet.